ELSEVIER

Engineering Analysis with Boundary Elements 28 (2004) 733–745

ENGINEERING ANALYSIS *with* BOUNDARY ELEMENTS

www.elsevier.com/locate/enganabound

Evaluation of various schemes for quasi-static boundary element analysis of polymers

Stavros Syngellakis*, Jiangwei Wu

Computational Engineering and Design Group, School of Engineering Sciences, University of Southampton, Highfield, Southampton SO17 1BJ, UK

Received 6 October 2003; revised 12 January 2004; accepted 27 January 2004

Abstract

The behaviour of polymers under quasi-static load is analysed by various boundary element schemes. Linear viscoelasticity, for which the correspondence principle applies, is assumed. The problem is first solved in the Laplace transform domain with the time-dependent response determined by numerical inversion. A solution is also obtained directly in the time domain using fundamental solutions for unit step load excitation. Two alternative time-domain schemes, applied until recently only to dynamic problems, are adapted to quasi-static conditions. Both are based on a reciprocity relation involving Riemann convolutions and use fundamental solutions for a Dirac impulse excitation. The second of those schemes, however, uses only the Laplace transforms of these fundamental solutions, which are directly formed from the corresponding elasticity solutions and thus not specific to the viscoelastic model used. Rapid derivation of time-dependent fundamental solutions for general standard linear solids enhances the applicability of time domain methods. Computer codes based on the different algorithms are developed and applied to benchmark problems in order to assess their relative accuracy, versatility and efficiency. The various BEM predictions are generally consistent and reliable. The numerical instability of the last, so called, mixed method is minimised through appropriate choice of modelling parameters.

Keywords: Boundary element methods; Polymers; Linear viscoelasticity; Quasi-static analyses

1. Introduction

The demand of high quality materials in engineering design has led to an increasing use of polymers due to their high strength to weight ratio and to their corrosion resistance Although polymers offer these advantages over traditional metallic materials, their characteristic time-dependent behaviour may lead to excessive creep and/or failure. Thus, the study of long-term polymer component behaviour under various loading conditions is becoming increasingly important.

Polymers are materials behaving according to a constitutive model known as viscoelasticity, which accounts for the dependence of stress and strain on time. In order to study the response of viscoelastic solids to arbitrary, external, time-dependent loads, a numerical analysis is normally needed. Whereas the finite element method (FEM) remains the most popular numerical method for solid material analysis, more recently, the boundary element method (BEM) has been developed as an effective alternative for the solution of a wide range of problems. Although many studies on the application of BEM to static or dynamic viscoelastic problems can be found in the literature, a systematic assessment of the relative merits or limitations of the various possible schemes is apparently missing.

There are two established approaches to linear viscoelastic quasi-static analysis by the BEM. The first method [1] uses the correspondence principle to generate an associated elastic problem, which is solved in the Laplace transform domain and the result is inverted numerically so that the solution in the time domain is obtained. This numerical inversion adds to the computational cost and may have a detrimental effect on overall accuracy if not performed with care. The transform domain scheme has, however, the advantage of relying on the fundamental solutions of the corresponding elasticity problems, it is therefore, conceptually easy to combine it with various types of solid analyses and a wide range of material models.

* Corresponding author. Tel.: +44-23-8059-2844; fax: +44-23-8059-3230/4813.

E-mail address: ss@soton.ac.uk (S. Syngellakis).

0955-7997/$ - see front matter © 2004 Elsevier Ltd. All rights reserved.
doi:10.1016/j.enganabound.2004.01.008

The second, direct method [2] involves a formulation based on a boundary integral equation in the time domain. The BEM solution is obtained by a step-by-step time integration scheme. This direct time domain method could be more efficient than the transform domain method but requires the identification or determination of time-dependent fundamental solutions specific to the solid geometry and the adopted viscoelastic model. The need for such solutions has restricted the applicability of time domain BEM approaches.

A more recently proposed method [3] seems to combine the advantages of the previous two, solving the problem in the time domain but relying on the fundamental solutions in the Laplace domain. The application of this mixed method to dynamic problems raised some stability and accuracy issues, which have not been fully addressed.

This paper focuses on quasi-static BEM analyses of polymers by the two established schemes mentioned above as well as two alternative time-domain formulations, originally applied to dynamic problems only. Both new schemes are based on a reciprocity relation involving Riemann rather than Stieltjes convolutions and rely on fundamental solutions for Dirac delta function excitations. The second of those schemes is an extension of Schanz's mixed method [3] to quasi-static problems. Numerical techniques are proposed for the rapid derivation of time-dependent fundamental solutions for general standard linear solids (SLS) under both step (Heaviside) and Dirac impulse excitations. Thus polymer behaviour can be more accurately represented and the versatility of time domain methods is greatly enhanced.

Computer codes based on different algorithms are developed and applied to benchmark problems in order to assess their relative accuracy and efficiency. The degree of agreement between various BEM predictions and exact solutions is examined. The applicability of the mixed method to almost any material model is explored through an investigation into the parameters controlling its accuracy and stability. Schemes for possible extension of the methods to account for more complex viscoelastic models are briefly discussed.

2. Viscoelastic models

The constitutive equations of linear viscoelasticity are, in accordance with Boltzmann's principle, of hereditary integral type

$$\sigma_{ij} = G_{ijkl}(t)\varepsilon_{kl}(0) + \int_0^t G_{ijkl}(t-\tau)\frac{\partial \varepsilon_{kl}}{\partial \tau}\mathrm{d}\tau \tag{1}$$

where $\sigma_{ij}, \varepsilon_{ij}$ are the stress and small strain tensors, respectively, and $G_{ijkl}(t)$ the relaxation moduli in the general case of an anisotropic medium. Adopting the notation for the Stieltjes convolution of two functions [4], Eq. (1) can be more concisely written

$$\sigma_{ij} = G_{ijkl} * \mathrm{d}\varepsilon_{kl} \tag{2}$$

In the case of an isotropic medium characterised by the bulk and shear relaxation moduli $K(t)$ and $\mu(t)$, respectively, constitutive relations (2) are reduced to

$$s_{ij} = 2\mu(t) * \mathrm{d}\varepsilon_{ij}(t), \qquad \sigma_{kk} = 3K(t) * \mathrm{d}\varepsilon_{kk}(t) \tag{3}$$

where s_{ij} and e_{ij} are, respectively, the deviatoric stress and strain tensors. An alternative form to constitutive Eq. (3) is [4]

$$e_{ij} = J(t) * \mathrm{d}s_{ij}(t), \qquad \varepsilon_{kk} = B(t) * \mathrm{d}\sigma_{kk}(t) \tag{4}$$

where $J(t)$ and $B(t)$ are, respectively, the shear and bulk creep moduli.

A commonly used rheological model is the generalised SLS [5]. It can be formed by connecting in series a Hookean spring and N Kelvin models, or by connecting in parallel a spring and N Maxwell models. The resulting viscoelastic equations are of differential operator type

$$\begin{aligned} \sum_{n=0}^{N} p_n^s D^n s_{ij} &= \sum_{n=0}^{N} q_n^s D^n e_{ij}, \\ \sum_{n=0}^{N} p_n^d D^n \sigma_{kk} &= \sum_{n=0}^{N} q_n^d D^n \varepsilon_{kk} \end{aligned} \tag{5}$$

where D^n is an operator representing the nth time derivative and $p_n^s, q_n^s, p_n^d, q_n^d$, are material constants, which can be related to the elastic moduli and viscosities of the spring and individual Kelvin or Maxwell elements making up the SLS model [5]. The solution of differential Eq. (5) under relaxation or creep conditions leads to the determination of the time-dependent relaxation or creep moduli, respectively. Thus, Prony series expressions for shear relaxation

$$\mu(t) = \mu_0 + \sum_{j=1}^{n} \mu_i \exp\left(-\frac{t}{\tau_j}\right) \tag{6}$$

and shear creep

$$J(t) = J_0 + \sum_{j=1}^{n} J_j\left[1 - \exp\left(-\frac{t}{\lambda_j}\right)\right] \tag{7}$$

are obtained from the generalised Maxwell and Kelvin models, respectively.

3. Field equations

Introducing the small strain–displacement relations into the constitutive Eq. (1) and substituting the latter into the stress equations of equilibrium yields a system of integro-differential equations

$$G_{ijkl}(t)u_{k,lj}(0) + \int_0^t G_{ijkl}(t-\tau)\frac{\partial u_{k,lj}}{\partial \tau}\mathrm{d}\tau + f_i = 0 \tag{8}$$

where f_i is the body force per unit volume. The problem is complemented by the boundary conditions

$$u_i(t) = \tilde{u}_i(t) \text{ on } \Gamma_1 \qquad \sigma_{ij}(t)n_j = \tilde{p}_i(t) \text{ on } \Gamma_2 \tag{9}$$

where $\tilde{u}_i(t)$ and $\tilde{p}_i(t)$ are, respectively, prescribed boundary values of the displacement and traction while $\mathbf{n}$ is the outward unit normal vector to the boundary $\Gamma = \Gamma_1 + \Gamma_2$.

Given two viscoelastic states (u_i, p_i, f_i) and (u_i^*, p_i^*, f_i^*), satisfying the boundary value problem described above, the reciprocal relation [4]

$$\int_\Gamma p_i * \mathrm{d}u_i^* \,\mathrm{d}\Gamma + \int_\Omega f_i * \mathrm{d}u_i^* \,\mathrm{d}\Omega = \int_\Gamma u_i * \mathrm{d}p_i^* \,\mathrm{d}\Gamma + \int_\Omega u_i * \mathrm{d}f_i^* \,\mathrm{d}\Omega \tag{10}$$

can be derived. The validity of the alternative reciprocity principle

$$\int_\Gamma p_i * u_i^* \,\mathrm{d}\Gamma + \int_\Omega f_i * u_i^* \,\mathrm{d}\Omega = \int_\Gamma u_i * p_i^* \,\mathrm{d}\Gamma + \int_\Omega u_i * f_i^* \,\mathrm{d}\Omega \tag{11}$$

involving Riemann rather than Stieltjes convolutions can be similarly proved.

4. Correspondence principle

Taking the Laplace transform of both sides of constitutive Eq. (1) gives

$$\bar{\sigma}_{ij} = s\bar{G}_{ijkl}\bar{\varepsilon}_{kl} = G^{\mathrm{L}}_{ijkl}\bar{\varepsilon}_{kl} \tag{12}$$

where s is the Laplace domain parameter and a bar over a symbol indicates the transform of the corresponding variable. By transforming also the equations of equilibrium (8), the strain–displacement relations, as well as the boundary conditions (9), a complete correspondence is established between the elastic and viscoelastic problem. Thus a linear viscoelastic problem can be solved in the transform domain for any range of values of the transform variable s by the same methods as those applicable to the corresponding elasticity problem in which the field variables are replaced by their Laplace transforms and the elastic constants are replaced by their equivalent functions according to Eq. (12). In the end, it is, of course, necessary to invert the transforms so obtained to solutions in real time. This, so called, correspondence principle has been applied to generate BEM solutions in the transform domain but also to obtain the fundamental solutions for particular viscoelastic models, which are subsequently used in BEM time domain formulations.

Taking the Laplace transform of both sides of Eq. (3) and introducing the Young's modulus E_{L} and Poisson's ratio ν_{L} in the transform domain, the relations

$$2s\bar{\mu} = \frac{E_{\mathrm{L}}}{1+\nu_{\mathrm{L}}}, \quad 3s\bar{K} = \frac{E_{\mathrm{L}}}{1+2\nu_{\mathrm{L}}} \tag{13}$$

are valid according to the correspondence principle. Thus, time-dependent uniaxial tension or compression modulus $E(t)$ and Poisson's ratio $\nu(t)$ can be obtained as the inverse Laplace transforms of the relations

$$E_{\mathrm{L}} = s\bar{E} = \frac{9s\bar{\mu}\bar{K}}{(\bar{\mu}+3\bar{K})}, \quad \nu_{\mathrm{L}} = s\bar{\nu} = \frac{3\bar{K}-2\bar{\mu}}{2(3\bar{K}+\bar{\mu})} \tag{14}$$

The correspondence principle can also be applied to determine creep moduli from respective relaxation moduli and vice versa.

5. BEM formulations

5.1. Laplace transform domain

If the correspondence principle is applied to a quasi-static problem, a BEM solution can be developed from the boundary integral equation in the Laplace transform domain

$$\kappa_{ij}\bar{\mu}_i = \int_\Gamma [\bar{p}_i(s)u_{ij}^*(s) - \bar{u}_i(s)p_{ij}^*(s)]\mathrm{d}\Gamma + \int_\Omega \bar{f}_i u_{ij}^* \,\mathrm{d}\Omega \tag{15}$$

where $\kappa_{ij} = 0.5\delta_{ij}$ in the case of a smooth boundary, and (u_{ij}^*, p_{ij}^*) is the elastic fundamental solution for displacements and tractions in which, however, the elastic constants have been replaced by the corresponding functions in the transform space according to Eq. (12) or Eq. (14). The calculated Laplace transforms of boundary or domain variables can be numerically inverted back to time-dependent functions using any of the available numerical inversion methods.

5.2. Time domain—Stieltjes convolution

In this case, the boundary integral equation can be obtained directly from the reciprocal relation of linear viscoelasticity, Eq. (10). This is achieved by choosing the system (u_i^*, p_i^*, f_i^*) to coincide with the fundamental solution of the viscoelastic problem, that is, the displacements u_{ij}^* and tractions p_{ij}^* generated by step unit body forces

$$f_{ij}^* = \delta_{ij}\delta(\mathbf{x} - \xi)H(t)$$

where δ_{ij} is the Kronecker delta, $\delta(\mathbf{x} - \xi)$ the delta function and the Heaviside step function. For a point ξ in the interior of Ω, Eq. (10) then becomes,

$$u_j(\xi, t) = \int_\Gamma [p_i(\mathbf{x}, t) * \mathrm{d}u_{ij}^*(\mathbf{x}, \xi; t) - u_i(\mathbf{x}, t) * \mathrm{d}p_{ij}^*(\mathbf{x}, \xi; t)]\mathrm{d}\Gamma + \int_\Omega f_i(\mathbf{x}, t) * \mathrm{d}u_{ij}^*(\mathbf{x}, \xi; t)\mathrm{d}\Omega \tag{16}$$

By taking the source point ξ in Eq. (16) to the boundary, the boundary integral equation in space and time is derived as

$$\kappa_{ij}u_i(t) = \int_\Gamma (p_i * \mathrm{d}u_{ij}^* - u_i * \mathrm{d}p_{ij}^*)\mathrm{d}\Gamma + \int_\Omega f_i * \mathrm{d}u_{ij}^* \,\mathrm{d}\Omega \tag{17}$$

Taking into account a property of the Stieltjes convolution [4], the boundary integral Eq. (17) is transformed to

$$\kappa_{ij}u_i(t) = \int_\Gamma (u^*_{ij} * \mathrm{d}p_i - p^*_{ij} * \mathrm{d}u_i)\mathrm{d}\Gamma + \int_\Omega f_i * \mathrm{d}u^*_{ij}\,\mathrm{d}\Omega \qquad (18)$$

The fundamental solution required in the above time domain formulation can be obtained by an inverse Laplace transform operation. This has been carried out in several special cases but also for general Kelvin or Maxwell SLS models [5].

5.3. Time domain—Riemann convolution

The fundamental solution $[u^*_{ij}(\mathbf{x}-\xi,t), p^*_{ij}(\mathbf{x}-\xi,t)]$, due to the Dirac unit impulse

$$f^*_{ij} = \delta_{ij}\delta(\mathbf{x}-\xi)\delta(t) \qquad (19)$$

is introduced as one of the viscoelastic states into the reciprocal relation (11). This leads to

$$\kappa_{ij} * u_i(t) = \int_\Gamma (u^*_{ij} * p_i - p^*_{ij} * u_i)\mathrm{d}\Gamma + \int_\Omega f_i * u^*_{ij}\,\mathrm{d}\Omega \qquad (20)$$

that is, an alternative boundary integral equation in the time domain. The convolution in the right-hand side of Eq. (20) is due to the possible dependence of κ_{ij} on the Poisson's ratio, which, in turn, may be time-dependent. As in the previous time domain formulation, the fundamental solution is obtained by applying the correspondence principle and inverse Laplace transform. A relatively simple procedure for evaluating the parameters of the time-dependent parts of the fundamental solutions for both Heaviside and Dirac excitations is described in Appendix A.

5.4. Mixed formulation

A special scheme, originally applied to dynamic problems [3], combines time domain integration with the Laplace transforms of the fundamental solutions This scheme is based on boundary integral Eq. (20) in which convolution integrals are approximated by a quadrature originally proposed by Lubich [6,7]. This approximation is briefly outlined in Appendix B. If time t_K is divided into K equal intervals Δt so that $t_K = K\Delta t$, a convolution integral, such as $u^*_{ij} * p_i$, in Eq. (20) may be approximated by

$$u^*_{ij}(\mathbf{x},\xi;t_n) * p_j(\mathbf{x},t_n) \cong \sum_{k=0}^{n} \omega^{n-k}_{ij}(\mathbf{x},\xi;\Delta t)p_j(\mathbf{x},k\Delta t);$$

$$n = 0,1,\ldots,K$$

where the integration weights ω^n_{ij} depend only on the Laplace transform $\bar{u}^*_{ij}$ according to the general relationships (B3) or (B4) given in Appendix B. Thus a time stepping procedure can be formulated directly in the time domain, although only the Laplace transforms of the fundamental solutions are used, that is, a viscoelastic boundary element formulation is achieved in the time domain without requiring the knowledge of the relevant time-dependent fundamental solution.

6. Boundary element modelling

Constant boundary elements with mid-element nodes were used in the present BEM formulations in both the transform and time domain. Thus, over an element Γ_e, the following approximation is adopted

$$u_j(\mathbf{x},t) = u^e_i(t), \qquad p_j(\mathbf{x},t) = p^e_j(t) \qquad (21)$$

where $u^e_j(t)$ and $p^e_j(t)$ are the time-dependent nodal values of displacement and traction, respectively. A BEM solution for the Laplace transforms of $u^e_j(t)$ and $p^e_j(t)$ is based on boundary integral Eq. (15) and thus proceeds in exactly the same manner as the corresponding elastic problem.

Time domain formulations based on integral Eqs. (17), (18) or (20) require also modelling of time dependence as well as a suitable choice of material model. It was assumed that the boundary variables $u_i(x,t)$ and $p_i(x,t)$ are linear with respect to time t within a small time step $\Delta t_\kappa = t_\kappa - t_{\kappa-1}$. The general SLS model was adopted since through it, polymer behaviour can be described with sufficient accuracy. It is shown in Appendix A, how fundamental solutions for this model can be obtained when relaxation functions are given by expressions in the form of Eq. (6). The time domain formulations were thus based on the viscoelastic fundamental solutions given by Eqs. (A15) and (A17).

Assuming zero body forces, boundary integral Eq. (18) was thus transformed to

$$\begin{aligned}\kappa_{ij}(\xi)u^{(K)}_i(\xi) = {} & \sum_{n=0}^{N} U^{n(K)}_j(\xi) + \sum_{\kappa=1}^{K}\sum_{n=1}^{N} U^{n(\kappa-1)}_j(\xi) \\ & \times\exp[-\beta_n(t_K - t_\kappa)][(\exp(-\beta_n\Delta t_\kappa) - 1] \\ & - \sum_{m=0}^{M} P^{m(K)}_j(\xi) - \sum_{\kappa=1}^{K}\sum_{m=1}^{M} P^{m(\kappa-1)}_j(\xi) \\ & \times\exp[-\alpha_m(t_K - t_\kappa)][(\exp(-\alpha_m\Delta t_\kappa) - 1]\end{aligned} \qquad (22)$$

where

$$u^{(\kappa)}_i(\mathbf{x}) = u_i(\mathbf{x},t_\kappa)$$

$$p^{(\kappa)}_i(\mathbf{x}) = p_i(\mathbf{x},t_\kappa)$$

$$P^{m(\kappa)}_j(\xi) = \int_\Gamma p^m_{ij}(\mathbf{x},\xi)u^{(\kappa)}_i(\mathbf{x})\mathrm{d}\Gamma = \sum_{e=1}^{E} u^{e(\kappa)}_i \int_{\Gamma_e} p^m_{ij}(\mathbf{x},\xi)\mathrm{d}\Gamma$$

$$U^{n(\kappa)}_j(\xi) = \int_\Gamma u^n_{ij}(\mathbf{x},\xi)p^{(\kappa)}_i(\mathbf{x})\mathrm{d}\Gamma = \sum_{e=1}^{E} p^{e(\kappa)}_i \int_{\Gamma_e} u^n_{ij}(\mathbf{x},\xi)\mathrm{d}\Gamma$$

with E representing the number of boundary elements and $u_{ij}^{n}(\mathbf{x},\xi),p_{ij}^{m}(\mathbf{x},\xi)$ the spatial parts of the fundamental solutions as defined in Appendix A. Placing the source point at each boundary node results in the matrix equation

$$\begin{aligned}\mathbf{C}\mathbf{u}^{(K)}=&\sum_{n=0}^{N}\mathbf{U}^{n(K)}\mathbf{p}^{(K)}+\sum_{\kappa=1}^{K}\left\{\sum_{n=1}^{N}\mathbf{U}^{n(\kappa-1)}\exp[-\beta_n(t_K-t_\kappa)]\right.\\&\left.\times[(\exp(-\beta_n\Delta t_\kappa)-1]\right\}\mathbf{p}^{(\kappa)}-\sum_{m=0}^{M}\mathbf{P}^{m(K)}\mathbf{u}^{(K)}\\&-\sum_{\kappa=1}^{K}\left\{\sum_{m=1}^{M}\mathbf{P}^{m(\kappa-1)}\exp[-\alpha_m(t_K-t_\kappa)]\right.\\&\left.\times[(\exp(-\alpha_m\Delta t_\kappa)-1]\right\}\mathbf{u}^{(\kappa)}\end{aligned}\tag{23}$$

where $\mathbf{u}^{(\kappa)}$ and $\mathbf{p}^{(\kappa)}$ are one-dimensional arrays containing, respectively, the nodal values of boundary displacement and traction at time t_κ. It is evident from Eq. (23) that the boundary displacements and tractions can be determined at any time $t=t_K$ if they are known at all previous times. At $t=0$, the boundary integral Eq. (17) governs only the initial elastic response due to any non-zero initial values of the boundary or loading conditions. At any other time $t=t_\kappa$ (step κ), the respective unknown boundary values can be obtained from Eq. (23) with the current boundary conditions and the additional terms depending only on the solution at the previous steps. A step-wise procedure is thus established which advances the solution until the final time step is reached.

After the unknown boundary values of the linear viscoelastic problem are determined, the displacements and stresses at internal points can be calculated. Internal displacements can be determined from Eq. (22) having set $\kappa_{ij}=\delta_{ij}$. The expressions giving the internal stresses in terms of the boundary displacements and tractions are

$$\begin{aligned}\sigma_{ij}(\xi,t)=&\int_\Gamma D_{kij}^{*}(\mathbf{x},\xi;t)*\mathrm{d}p_k(\mathbf{x},t)\mathrm{d}\Gamma\\&-\int_\Gamma S_{kij}^{*}(\mathbf{x},\xi;t)*\mathrm{d}u_k(\mathbf{x},t)\mathrm{d}\Gamma\\&+\int_\Omega f_k(\mathbf{x},t)*\mathrm{d}D_{kij}^{*}(\mathbf{x},\xi;t)\mathrm{d}\Omega\end{aligned}\tag{24}$$

As mentioned earlier, the time-dependent stress kernels appearing on the right hand-side of Eq. (24) can be derived from the respective elastic stress kernels by applying the correspondence principle and inverting the resulting equations from the transform domain to real time domain.

The same modelling was applied to the boundary integral Eq. (20) based on the reciprocity relation (11) and Dirac unit impulse. In the case of constant boundary elements, the source point is never a corner point, therefore the convolution on the right-hand side of Eq. (20) can be ignored. Linear time dependence of boundary variables over Δt results in more complex expressions for the convolution integrals than in the previous formulation, which involved time derivatives of the displacement and traction. These expressions are considerably simplified if a small, constant time step Δt is adopted. With this simplification and body forces ignored, Eq. (20) is transformed into the following matrix equation

$$\begin{aligned}\mathbf{C}\mathbf{u}^{(K)}=&\left(\mathbf{U}^0+\frac{\Delta t}{2}\sum_{n=1}^{N}\mathbf{U}^n\right)\mathbf{p}^{(K)}\\&+\Delta t\sum_{\kappa=1}^{K}\left\{\sum_{n=1}^{N}\mathbf{U}^n\exp[-\beta_n(K-\kappa)\Delta t]\right\}\mathbf{p}^{(\kappa)}\\&-\frac{\Delta t}{2}\left[\sum_{n=1}^{N}\mathbf{U}^n\exp(-\beta_nK\Delta t)\right]\mathbf{p}^{(0)}\\&-\left(\mathbf{P}^0+\frac{\Delta t}{2}\sum_{m=1}^{M}\mathbf{P}^m\right)\mathbf{u}^{(K)}\\&-\Delta t\sum_{\kappa=1}^{K-1}\left\{\sum_{m=1}^{M}\mathbf{P}^m\exp[-\alpha_m(K-\kappa)\Delta t]\right\}\mathbf{u}^{(\kappa)}\\&-\frac{\Delta t}{2}\left[\sum_{m=1}^{M}\mathbf{P}^m\exp(-\alpha_mK\Delta t)\right]\mathbf{u}^{(0)}\end{aligned}$$

which can be solved by the same time-step procedure as that applied to Eq. (23).

Finally, the numerical algorithm for the mixed method is obtained by inserting the boundary models (21) in Eq. (20) assuming no source points at corners and zero body forces. This gives

$$\begin{aligned}\kappa_{ij}u_i(t)=&\sum_{e=1}^{E}\left[\int_{\Gamma_e}u_{ij}^{*}(\mathbf{x},\xi;t)*p_j^{e}(t)\mathrm{d}\Gamma\right.\\&\left.-\int_{\Gamma_e}p_{ij}^{*}(\mathbf{x},\xi;t)*u_j^{e}(t)\mathrm{d}\Gamma\right]\end{aligned}\tag{25}$$

Applying the quadrature formula proposed by Lubich to the integral Eq. (25) results in the following boundary element time-stepping formulation for $n=0,1,\ldots,K$,

$$\begin{aligned}\kappa_{ij}u_i(t_n)=&\sum_{k=0}^{n}\sum_{e=1}^{E}\left[\Omega_{ij}^{e,n-k}(\xi,\Delta t)p_j^{e}(k\Delta t)\right.\\&\left.-\Phi_{ij}^{e,n-k}(\xi,\Delta t)u_j^{e}(k\Delta t)\right]\end{aligned}\tag{26}$$

with the spatial integration incorporated into the weights $\Omega_{ij}^{e,n}$ and $\Phi_{ij}^{e,n}$ according to

$$\Omega_{ij}^{e,n}(\xi,\Delta t)=\frac{1}{L}\sum_{l=0}^{L-1}\zeta_l^{-n}\int_{\Gamma_e}\bar{u}_{ij}^{*}\left[\mathbf{x},\xi;\frac{\gamma(\zeta_l)}{\Delta t}\right]\mathrm{d}\Gamma(\mathbf{x})\tag{27}$$

$$\Phi_{ij}^{e,n}(\xi,\Delta t)=\frac{1}{L}\sum_{l=0}^{L-1}\zeta_l^{-n}\int_{\Gamma_e}\bar{p}_{ij}^{*}\left[\mathbf{x},\xi;\frac{\gamma(\zeta_l)}{\Delta t}\right]\mathrm{d}\Gamma(\mathbf{x})\tag{28}$$

and all parameters appearing in the above expressions defined in Appendix B. All convolutions were approximated using the third-order backward differentiation formula, that is, with $P=3$ in Eq. (B2). Recalling that the spatial and time

dependence of the fundamental solutions can be separated according to Eq. (A1), expression (27) can be simplified to

$$\Omega_{ij}^{e,n}(\xi,\Delta t) = a_n(\Delta t)F_{ij}^e(\xi) + b_n(\Delta t)G_{ij}^e(\xi)$$

where

$$F_{ij}^e(\xi) = \int_{\Gamma_e} f_{ij}(\mathbf{x},\xi)\mathrm{d}\Gamma(\mathbf{x}), \qquad G_{ij}^e(\mathbf{x}) = \int_{\Gamma_e} g_{ij}(\mathbf{x},\xi)\mathrm{d}\Gamma(\mathbf{x})$$

and

$$a_n(\Delta t) = \frac{1}{L}\sum_{l=0}^{L-1} \zeta_l^{-n}\bar{A}\left[\frac{\gamma(\zeta_l)}{\Delta t}\right],$$

$$b_n(\Delta t) = \frac{1}{L}\sum_{l=0}^{L-1} \zeta_l^{-n}\bar{B}\left[\frac{\gamma(\zeta_l)}{\Delta t}\right]$$

The expression for $\Phi_{ij}^{e,n}$ can be simplified in a similar manner. The algebraic system of Eq. (26) can be solved for successive values of n, starting from $n = 0$, that is, the solution at $t = 0$.

The algorithms described in this section were implemented through MATLAB and FORTRAN programs. Comparison of MATLAB and FORTRAN outputs provided an additional check on the accuracy of programming. MATLAB was found more user-friendly but also slower than FORTRAN. In anticipation of complex applications of viscoelastic analysis involving repeated calculations or iterative schemes, robust and fully validated FORTRAN programs were developed for all formulations from which all results presented in Section 7 were obtained.

7. Numerical results and discussion

7.1. Comparison of the methods

The accuracy and effectiveness of the schemes described in Section 5 was assessed through the benchmark problem shown in Fig. 1 A thick wall cylinder under uniform internal pressure $p(t)$ over its inner boundary L_1 (radius a) is reinforced by an elastic ring at its outer boundary L_0 (radius b). Initially, no traction or gap is assumed between the cylinder and the ring. Provided the edges of the cylinder are fixed, radial traction and displacement at the outer boundary satisfy the relation

$$p_r(b,t) = -\frac{Eh}{(1-\nu^2)b^2}u_r(b,t)$$

where h is the thickness, E, the Young's modulus and ν, the Poisson's ratio of the elastic ring. The same problem was solved in previous independent assessments of Laplace transform [1] and time domain [8] schemes.

The numerical values used for the various parameters were: $a = 6$, $b = 20$, $h = 1$ mm, $E = 207$ GPa, and $\nu = 0.25$. A step load $p = 100$ MPa was applied at time $t = 0$. The adopted viscoelastic material model bore some

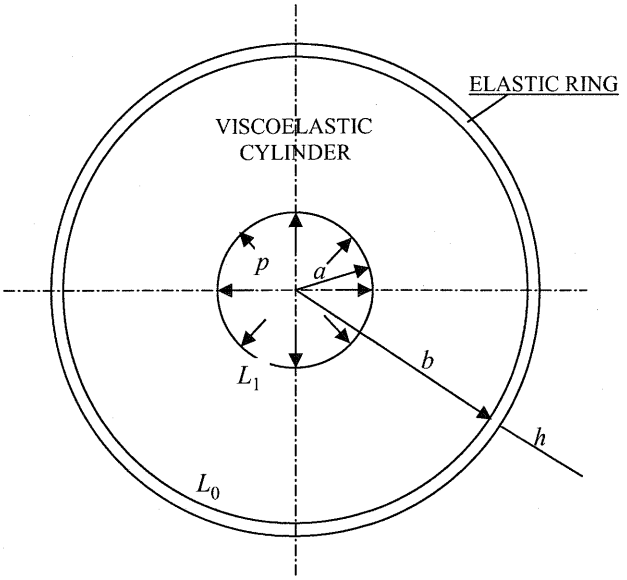

Fig. 1. Thick wall cylinder reinforced by an elastic ring.

resemblance to a real polymer as reported in the literature [9] namely, elastic in bulk deformation with $K = 2070$ MPa and viscoelastic in shear. A rough three-term Prony series approximation was fitted to the experimental creep data and subsequently converted to the shear relaxation modulus

$$\mu(t) = 609.90 + 118.79\,\mathrm{e}^{-0.00125t} + 57.494\,\mathrm{e}^{-5.372t} + 27.346\,\mathrm{e}^{-1.725t}(\mathrm{MPa}) \tag{29}$$

The fundamental solutions as well as the exact solution of this problem, corresponding to the adopted viscoelastic model, were derived for both plane strain and plane stress conditions, by applying the correspondence principle to the associated elastic solutions.

Taking advantage of symmetry, only one quarter of the cylinder was analysed. Meshing and symmetry conditions were applied along internal boundaries so that circumferential stresses and radial displacements could be obtained directly from the boundary solution. This strategy also led to a geometrically more complex and computationally more demanding problem for testing the developed algorithms. The three meshes used with all methods are shown in Figs. 2–4, where N_{BE} is the number of boundary elements. In the first two meshes, boundary elements of variable length were used along internal boundaries for improving accuracy around corners. All methods were applied with the time step kept constant at $\Delta t = 50$ s. In the transform method, time histories were obtained by Schapery's inversion method [1]. The mixed method was applied with $N = 150$, $L = 80$ and $\rho = 0.95$.

Tables 1–3 show the average error for all three boundary element meshes and the time step adopted. It can be observed first that the Laplace transform and the two time domain methods produce extremely consistent results. The accuracy of the mixed method is generally close to

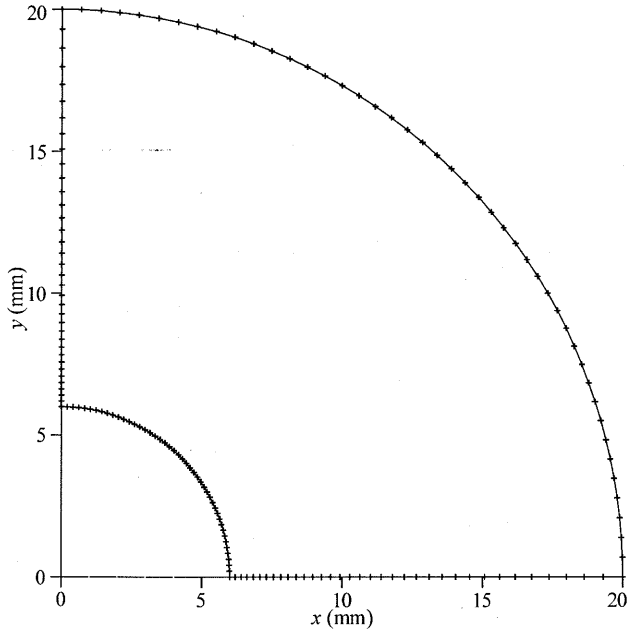

Fig. 2. Boundary element mesh with $N_{BE} = 160$.

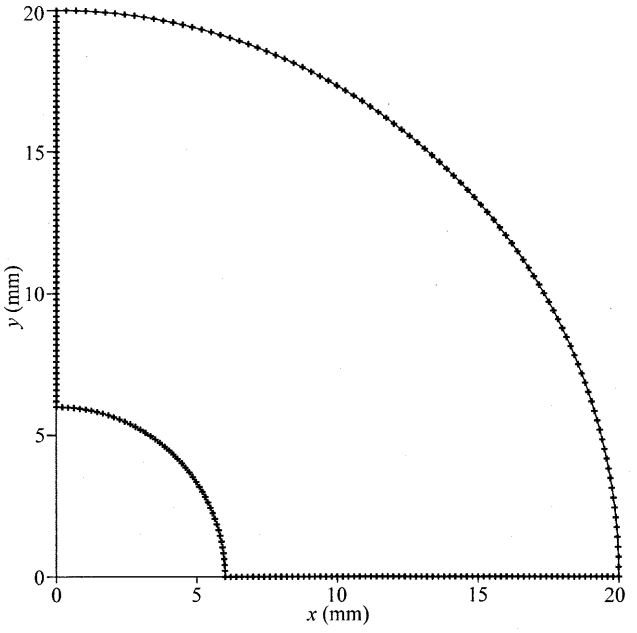

Fig. 4. Boundary element mesh with $N_{BE} = 275$.

that of the other three apart from certain initial values. In such cases, better agreement between methods can be linked to smaller element size. Most results are in very good agreement with the exact analytical solution. Large percentage errors are only noted at locations where the actual value of the result is very small. The accuracy of the results clearly depends on the element size but also on the proximity of the calculation point to a corner. This suggests refining the mesh around corners as well as increasing the number of boundary elements for improving accuracy. Tables 1–3 are based on results obtained under plane strain conditions but analyses performed under plane stress gave results with very similar trends.

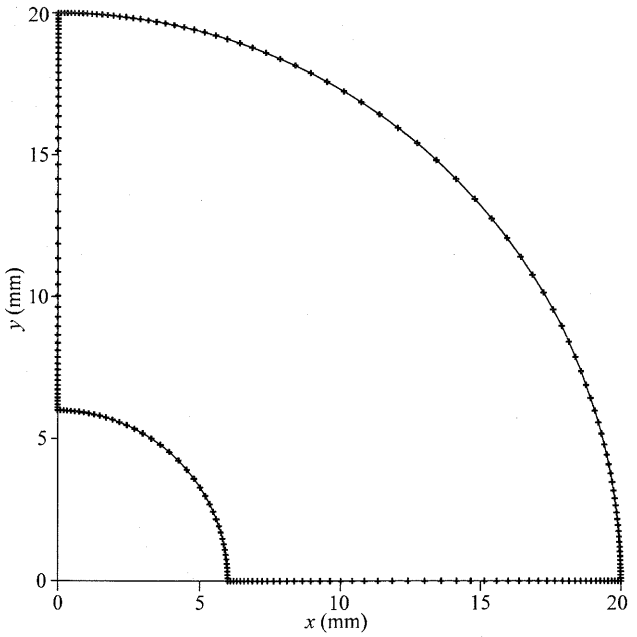

Fig. 3. Boundary element mesh with $N_{BE} = 220$.

The mixed method provided a stable solution for up to 4000 s. Beyond this time, the solution began to oscillate until, eventually, becoming highly unstable. For this reason, no mixed method results for $t = 5000$ s are given in the tables. Increasing the time step to $\Delta t = 100$ s prolonged the stable solution time but did not remove the instability problem, which is further investigated in Section 7.2. This time step change did not have any noticeable effect on the absolute or relative accuracies of all other methods.

7.2. Assessment of the mixed method

The convergence problems associated with the mixed method prompted further investigation into the effects of parameters that may affect performance. The geometry and loading of the analysed example were the same as those described in Section 7.1, but the material model slightly simpler, i.e. SLS in shear according to

$$\mu(t) = 12 + 36\,\mathrm{e}^{-0.4t}(\mathrm{GPa}) \tag{30}$$

and elastic in bulk deformation with $K = 128$ GPa, as previously adopted for the same problem [8]. Plane strain conditions were again assumed. A coarser uniform mesh consisting of 88 boundary elements was adopted to increase computational efficiency since the focus here was on solution convergence rather than accuracy.

The effect of the time step Δt on accuracy was first examined and found to be significant. In contrast, however, to the direct time domain method, reducing Δt did not necessarily improve the results. The optimum Δt value is apparently linked to the boundary element size as already

Table 1
Comparison of the methods based on circumferential stress at various times and locations ($N_{BE} = 160$, $\Delta t = 50$ s)

$(r-a)/(b-a)$	Time (s)	Exact solution (MPa)	Relative error (%)			
			Laplace domain	Time domain (Heaviside)	Time domain (Dirac)	Mixed method
0.007	0	70.336	1.58	1.58	1.58	1.36
	1000	67.557	1.51	1.54	1.50	1.45
	3500	66.230	1.48	1.49	1.48	1.51
	5000	66.140	1.49	1.49	1.48	N/A
0.037	0	60.002	−0.62	−0.62	−0.62	−0.84
	1000	57.392	−0.62	−0.61	−0.62	−0.68
	3500	56.146	−0.62	−0.62	−0.62	−0.62
	5000	56.061	−0.62	−0.62	−0.62	N/A
0.558	0	2.923	−1.64	−1.64	−1.64	−4.68
	1000	1.244	−3.97	−4.03	−4.00	−5.80
	3500	0.442	−11.35	−11.33	−11.42	−11.89
	5000	0.388	−12.60	−12.90	−13.04	N/A
0.975	0	−5.354	5.49	5.49	5.49	7.03
	1000	−6.898	4.39	4.39	4.40	4.70
	3500	−7.634	4.00	4.00	4.01	4.01
	5000	−7.685	3.96	3.98	3.99	N/A

pointed out in applications of the method to dynamic problems [3]. Whatever the choice of the Δt, it was never possible to achieve a stable solution over the whole predefined total time $t_K = K\Delta t$. The stability of the method was measured in terms of the percentage of this total time during which the solution remained stable. First, parameter L was varied from 20 to 100, while ρ and K remained constant at 0.85 and 101, respectively. The larger the L, the greater was the proportion of stable solution time, which reached 62% of t_K for certain results but improved only marginally for further increases of L. The effect of parameter ρ was also examined keeping L, K and Δt constant at 50, 101 and 0.5 s, respectively. The closer the value of ρ to unity, the longer was the stable solution time but again it only reached 49% of t_K for $\rho = 0.95$.

Since Δt affects only the accuracy but not the stability of the solution, it is possible to achieve results over a longer period by adopting different values of Δt. This is demonstrated in Fig. 5 where the circumferential stress at $r = 13.5$ mm is plotted versus time. The solution with $\Delta t = 1$ s is clearly more accurate than that obtained using $\Delta t = 5$ s but diverges at around 50 s. The solution with

Table 2
Comparison of the methods based on circumferential stress at various times and locations ($N_{BE} = 220$, $\Delta t = 50$ s)

$(r-a)/(b-a)$	Time (s)	Exact solution (MPa)	Relative error (%)			
			Laplace domain	Time domain (Heaviside)	Time domain (Dirac)	Mixed method
0.004	0	71.726	2.52	2.52	2.52	2.30
	1000	68.924	2.35	2.39	2.34	2.29
	3500	67.587	2.28	2.29	2.27	2.24
	5000	67.496	2.28	2.28	2.27	N/A
0.011	0	68.876	−0.53	−0.53	−0.53	−0.75
	1000	66.121	−0.57	−0.56	−0.57	−0.62
	3500	64.806	−0.58	−0.58	−0.58	−0.60
	5000	64.717	−0.58	−0.58	−0.59	N/A
0.562	0	2.779	−3.46	−3.46	−3.46	−6.65
	1000	1.102	−8.64	−8.70	−8.67	−10.69
	3500	0.302	−31.41	−31.38	−31.52	−32.30
	5000	0.248	−37.75	−38.21	−38.42	N/A
0.989	0	−5.512	−0.58	−0.58	−0.58	0.91
	1000	−7.053	−0.29	−0.30	−0.28	0.01
	3500	−7.789	−0.20	−0.20	−0.19	−0.15
	5000	−7.839	−0.21	−0.20	−0.19	N/A
0.996	0	−5.594	−3.47	−3.47	−3.47	−1.98
	1000	−7.134	−2.24	−2.29	−2.24	−1.95
	3500	−7.869	−1.86	−1.87	−1.85	−1.77
	5000	−7.919	−1.85	−1.84	−1.83	N/A

Table 3
Comparison of the methods based on circumferential stress at various times and locations ($N_{BE} = 275$, $\Delta t = 50$ s)

$(r-a)/(b-a)$	Time (s)	Exact solution (MPa)	Relative error (%)			
			Laplace domain	Time domain (Heaviside)	Time domain (Dirac)	Mixed method
0.007	0	70.336	1.07	1.07	1.07	0.86
	1000	67.557	1.02	1.05	1.02	0.96
	3500	66.230	1.00	1.01	1.00	0.98
	5000	66.140	1.01	1.01	1.00	N/A
0.036	0	60.344	−0.74	−0.75	−0.75	−0.97
	1000	57.728	−0.74	−0.74	−0.75	−0.80
	3500	56.479	−0.74	−0.74	−0.75	−0.76
	5000	56.395	−0.74	−0.74	−0.75	N/A
0.536	0	3.677	−0.41	−0.41	−0.41	−2.85
	1000	1.985	−0.88	−0.32	−0.90	−2.03
	3500	1.178	−1.59	−1.58	−1.61	−1.81
	5000	1.123	−1.55	−1.65	−1.70	N/A
0.579	0	2.252	−0.69	−0.69	−0.69	−4.62
	1000	0.584	−3.06	−3.17	−3.12	−6.92
	3500	−0.212	8.98	8.93	9.13	10.24
	5000	−0.266	6.67	7.10	7.30	N/A
0.964	0	−5.228	1.08	1.08	1.08	2.65
	1000	−6.774	0.86	0.86	0.86	−1.45
	3500	−7.512	0.78	0.78	0.79	0.82
	5000	−7.562	0.76	0.77	0.78	N/A
0.993	0	−5.554	−0.65	−0.65	−0.65	0.84
	1000	−7.095	−0.23	−0.25	−0.22	0.07
	3500	−7.830	−0.11	−0.11	−0.10	−0.04
	5000	−7.880	−0.12	−0.11	−0.10	N/A

$\Delta t = 5$ s prolongs the stable solution time without significantly affecting accuracy at later times.

The performance of the mixed versus the time domain methods was also assessed in relation to the initial loading conditions. It was shown in Section 7.1 that for a step load at $t = 0$, the initial response was, in general, accurately predicted by all methods with the more severe discrepancies associated with the mixed method (see Tables 1–3). The applied internal pressure is here ramped from zero to its maximum value according to

$$p(t) = \begin{cases} at \text{ (MPa)}, & t \le 100/a \\ 100 \text{ MPa}, & t > 100/a \end{cases}$$

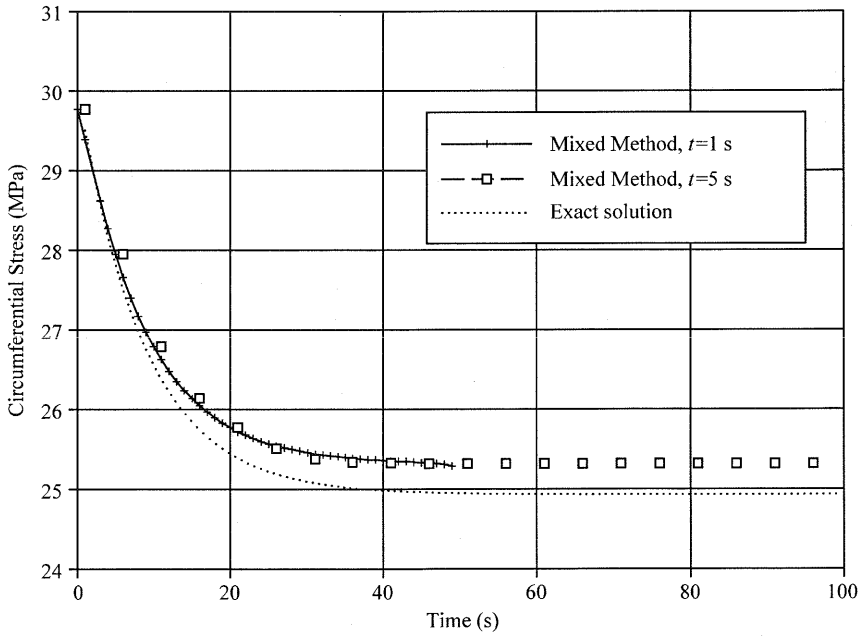

Fig. 5. Stress at $r = 13.5$ mm in thick wall cylinder under step loading.

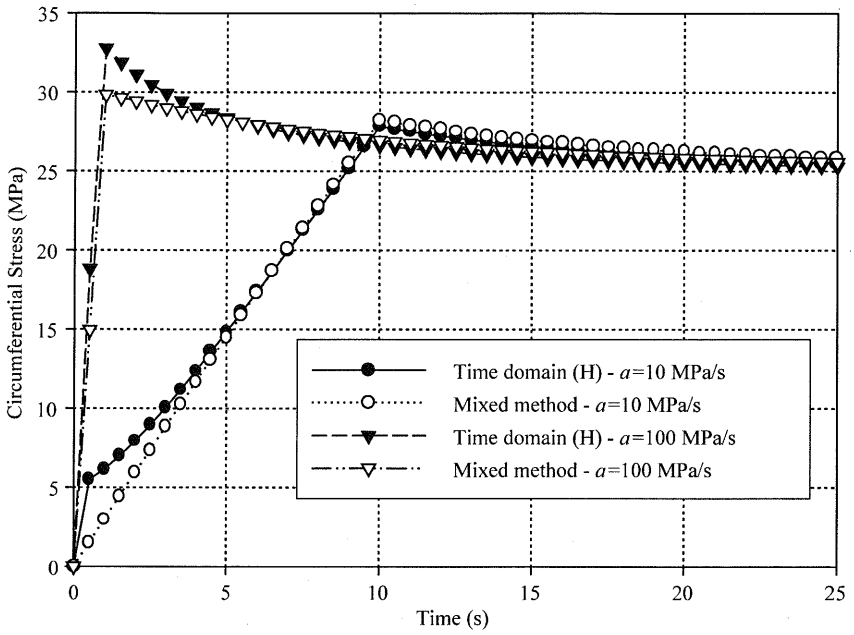

Fig. 6. Stress at $r = 13.5$ mm in thick wall cylinder under ramped loading.

The results for the circumferential stress at $r = 13.5$ mm, for two values of a, are shown in Fig. 6. It is seen that the mixed method captures very accurately the smooth initial stress variation in contrast to the time domain solution based on Stieltjes convolution, which appears to generate a significant initial deviation.

Finally, the mixed method was applied to a geometrically simpler example involving an infinite viscoelastic plate with a circular hole of 3 mm radius whose edge is subjected to a step pressure of 100 MPa at $t = 0$. The material model remained the same, i.e. with a shear relaxation modulus given by Eq. (30) and a constant bulk relaxation modulus $K = 128$ GPa. The critical parameter in this case was the number of boundary elements, which varied from 36 to 360. The values of the other input parameters were kept constant at $\Delta t = 0.5$ s, $K = 101$, $L = 50$ and $\rho = 0.85$. Fig. 7 shows the time variation of the radial displacement at $r = 50$ mm for two values of N_{BE}. The accuracy of the result is seen to improve with increasing number of boundary elements but with the stable solution time becoming gradually shorter. For $N_{BE} = 360$, the solution became unstable from the second solution step.

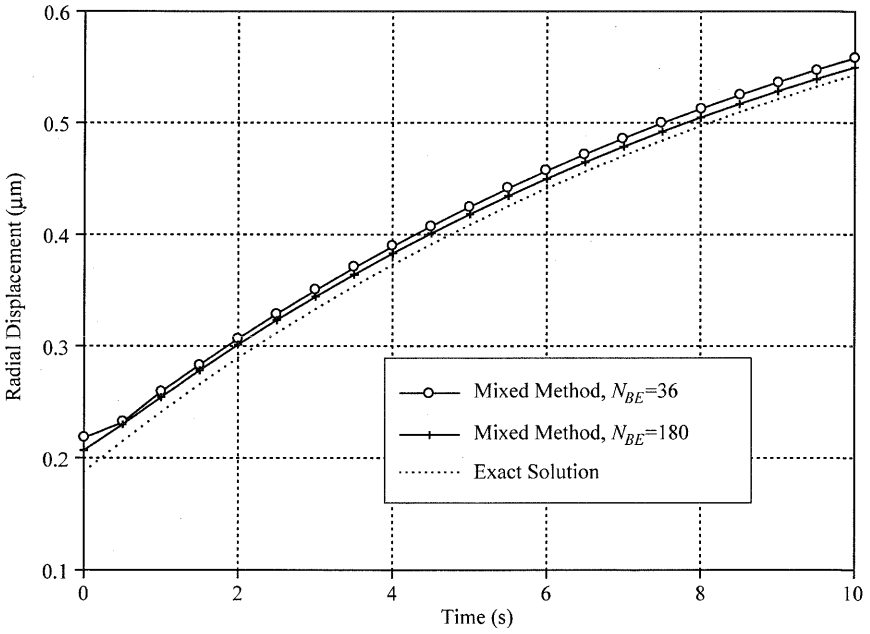

Fig. 7. Displacement at $r = 50$ mm in infinite space with a hole under step internal pressure.

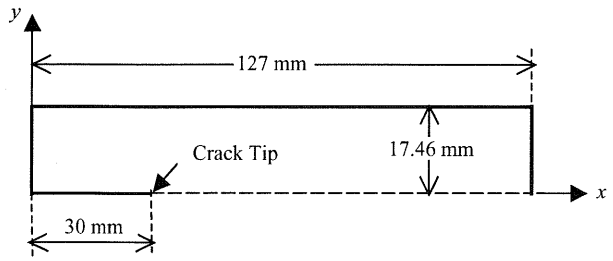

Fig. 8. Centrally cracked long strip.

7.3. Cracked strip

The performance of Laplace and time (Heaviside) domain methods was also compared in the case of a long strip with a central crack under uniform lateral extension This was a model of a specimen used for studying crack propagation in a viscoelastic solid [10]. Accounting for symmetry with respect to both x and y axes, only one quarter of the plate was analysed as shown in Fig. 8. The material was assumed to have a constant Poisson's ratio $\nu = 0.4$ and a SLS behaviour in shear

$$\mu(t) = 1.057 + 154.3\, e^{-5t}(\text{MPa}) \tag{31}$$

This material model represents only roughly the time dependence of the material tested by Mueller and Knauss [10] giving the quoted extreme values of relaxation modulus at $t = 0$ and $t = \infty$. A lateral extension $u_y = 0.2$ mm was uniformly applied along the edge $y = 17.46$ mm. The BEM model consisted of 534 boundary elements the majority of which were located in the neighbourhood of the crack tip.

The results for the time-dependent stress concentration factor $K_I(t)$ shown in Fig. 9 were obtained using

$$K_I(t) = \lim_{r\to 0} \sigma_{yy}(r,t)\sqrt{2\pi r} \tag{32}$$

where $r = x - 30$ (mm) is the distance from the crack tip. The limit on the right hand side of Eq. (32) was identified by linear regression since, theoretically, the corresponding expression can be approximated by a straight line near $r = 0$. Although the agreement between the two BEM solutions at $t = 0$ is very good, considerable deviation is observed at later times. This can be attributed to the choice of range and values for the Laplace transform parameter s. The extreme BEM time domain results $K_I(0) = 20.89$ and $K_I(\infty) = 0.1420$ N mm$^{-3/2}$ are comparable to the respective approximate theoretical predictions for an infinite strip $K_I(0) = 22.72$ and $K_I(\infty) = 0.1545$ N mm$^{-3/2}$ [10].

8. Discussion and conclusions

The transform domain method was shown to be as accurate as the time domain methods and is certainly more versatile since it can be adapted to any type of viscoelastic model. However, it requires the transform inversion and the associated choice of range and distribution of the transform parameter, both having a strong influence on the accuracy of the final results. This was more evident in the results of the cracked strip problem featuring singular, strongly time-dependent stress fields. Increasing the number of transform domain solutions imposes a heavy computational penalty on the final output especially when the solution needs to be applied iteratively.

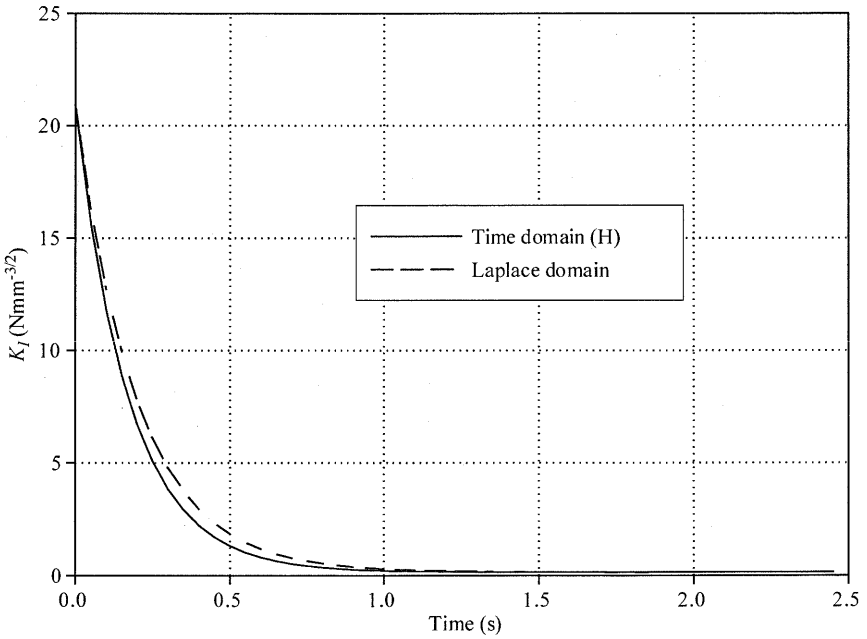

Fig. 9. Stress intensity factor for the strip problem.

The two time domain methods provide almost identical results and it is surprising that only that based on Stieltjes convolutions has so far found wide applicability among BEM developers at least for quasi-static problems. Since these methods yield directly time histories of results, they are potentially more efficient than the transform domain method. Another advantage of the time domain methods is that they can handle more easily inputs of complex time histories of boundary conditions. They are, therefore, a more rational choice for solving geometrically or materially non-linear problems. However, the time-dependent fundamental solution for the adopted viscoelastic model must be available. It was shown that such solutions can be generated with relative ease provided the material can be represented as a generalised SLS of either Kelvin or Maxwell type.

It is true, however, that more economical polymer modelling can be achieved using, for instance, fractional-order time derivatives. In such a case, it may be impossible to find a convenient form of the appropriate fundamental solution. This disadvantage can be overcome by applying the mixed method [3], which requires only the knowledge of the Laplace transform of the fundamental solution. The latter is easily obtained via the correspondence principle. Through applications to quasi-static problems, ranges of parameters guaranteeing the stability of the mixed method were identified. Initial assessments of its potential have shown that its accuracy and stability depend on appropriate choices of the approximation parameters Δt, ρ and L, as well as element size. The effect of these parameters should be explored further through applications to both quasi-static and dynamic problems before this method can be accepted as a valid versatile alternative to the other three in most practical cases.

There is considerable scope for increasing the potential of the BEM methods to solve complex viscoelastic problems. The first step would be to develop and test three-dimensional algorithms and then enhance their range of material modelling. This will extend their applicability to complex, industry-oriented problems. One such challenging area is fracture mechanics associated with geometry changes and high stress concentration possibly leading to the onset of non-linear viscoelastic behaviour, which would require additional modelling parameters and impose significant modifications to the existing BEM algorithms.

Appendix A. Time-dependent fundamental solutions for standard linear solids

The Laplace transform of the viscoelastic time-dependent fundamental solution due to a unit step or Dirac load can be written in the general form

$$\bar{u}^*_{ij}(s) = \bar{A}(s) f_{ij}(\mathbf{x} - \xi) + \bar{B}(s) g_{ij}(\mathbf{x} - \xi) \tag{A1}$$

where the spatial functions f_{ij} and g_{ij} are obtained from the corresponding elasticity solutions. For two-dimensional problems, they are given by

$$f_{ij} = -\frac{\delta_{ij} \ln r}{8\pi} \tag{A2}$$

$$g_{ij} = -\frac{r_{,i} r_{,j}}{8\pi} \tag{A3}$$

where $r = |\mathbf{x} - \xi|$. The functions $\bar{A}(s)$ and $\bar{B}(s)$ correspond to constant coefficients in the elastic solutions usually expressed in terms of the shear modulus and Poisson's ratio. If isotropic viscoelastic behaviour is characterised by the shear and bulk relaxation moduli, the appropriate expressions for $\bar{A}(s)$ and $\bar{B}(s)$ are obtained using Eq. (14) as follows,

(i) Plane strain

$$\bar{A}(s) = \frac{2[3\bar{K}(s) + 7\bar{\mu}(s)]}{s^\alpha \bar{\mu}(s)[3\bar{K}(s) + 4\bar{\mu}(s)]} \tag{A4}$$

$$\bar{B}(s) = \frac{2[3\bar{K}(s) + \bar{\mu}(s)]}{s^\alpha \bar{\mu}(s)[3\bar{K}(s) + 4\bar{\mu}(s)]} \tag{A5}$$

(ii) Plane stress

$$\bar{A}(s) = \frac{15\bar{K}(s) + 8\bar{\mu}(s)]}{2s^\alpha \bar{\mu}(s)[3\bar{K}(s) + \bar{\mu}(s)]} \tag{A6}$$

$$\bar{B}(s) = \frac{9\bar{K}(s)}{s^\alpha \bar{\mu}(s)[3\bar{K}(s) + \bar{\mu}(s)]} \tag{A7}$$

where $\bar{\mu}(s)$ and $\bar{K}(s)$ are the Laplace transforms of the viscoelastic shear and bulk relaxation moduli, respectively; $\alpha = 2$ for the fundamental solution due to a Heaviside step impulse; $\alpha = 1$ for that due to a Dirac delta impulse.

If expressions for viscoelastic bulk and shear relaxation moduli are adopted according to the generalised Maxwell SLS model, Eq. (6), their Laplace transforms would be given by

$$\bar{\mu}(s) = \frac{\mu_0}{s} + \sum_{j=1}^{P} \frac{\mu_j}{s + \tau_{\mu j}^{-1}} \tag{A8}$$

$$\bar{K}(s) = \frac{K_0}{s} + \sum_{j=1}^{Q} \frac{K_j}{s + \tau_{Kj}^{-1}} \tag{A9}$$

Substituting Eqs. (A8) and (A9) into Eq. (A6), gives expressions of the form

$$\bar{A}(s) = \frac{\sum_{j=0}^{N} a_j s^j}{s^{\alpha-1} \sum_{j=0}^{N} b_j s^j} = \frac{\gamma_0}{s^{\alpha-1}} + \sum_{j=1}^{N} \frac{\gamma_j}{s + \beta_j} \tag{A10}$$

where the coefficients a_j, b_j are functions of the material parameters μ_j, $\tau_{\mu j}$, K_j, τ_{Kj}, $N = 2P + Q$, and

$-\beta_1, -\beta_2, \ldots, -\beta_N$ are the N roots of an algebraic equation of degree N, $b_N s^N + b_{N-1}s^{N-1} + \ldots + b_1 s + b_0 = 0$.

If β_j are distinct, for $\alpha = 2$, the coefficients $\gamma_j (j = 0, 1, \ldots N)$ are determined from

$$\gamma_j = \lim_{s \to -\beta_j} \frac{(s+\beta_j)\sum_{k=0}^{N} a_k s^k}{s\sum_{k=0}^{N} b_k s^k} \tag{A11}$$

with $\beta_0 = 0$. For $\alpha = 1$, the coefficients γ_n are obtained from

$$\begin{cases} \gamma_0 = \dfrac{a_N}{b_N} \\ \gamma_j = \lim\limits_{s \to -\beta_j} \dfrac{(s+\beta_j)\sum_{k=0}^{N-1}\left[a_k - \dfrac{a_N}{b_N} b_k\right] s^k}{\sum_{k=0}^{N} b_k s^k} \end{cases} \tag{A12}$$

Thus the inverse transform of $\bar{A}(s)$ is,

$$A(t) = \gamma_0[\delta_{1\alpha}\delta(t) + \delta_{2\alpha}] + \sum_{n=1}^{N} \gamma_n \, \mathrm{e}^{-\beta_n t} \tag{A13}$$

The same procedure can be applied to Eq. (A7) to obtain the inverse transform of $\bar{B}(s)$, which has a similar form to that of $\bar{A}(s)$ given by Eq. (A10), but with a_n and χ_n replaced by different sets of coefficients d_n and γ_n, respectively, which are also functions of the material parameters. Making these substitutions into Eqs. (A11) and (A12), the inverse transform of $\bar{B}(s)$ can be obtained as

$$B(t) = \chi_0[\delta_{1\alpha}\delta(t) + \delta_{2\alpha}] + \sum_{n=1}^{N} \chi_n \, \mathrm{e}^{-\beta_n t} \tag{A14}$$

Substituting expressions (A13) and (A14) in the inverse transform of Eq. (A1), the viscoelastic fundamental solution for the displacement due to either a Dirac ($\alpha = 1$) or a Heaviside ($\alpha = 2$) step impulse is obtained as

$$u_{ij}^{*}(\mathbf{x}, \xi; t) = [\delta_{1\alpha}\delta(t) + \delta_{2\alpha}]u_{ij}^{0}(\mathbf{x}, \xi) + \sum_{n=1}^{N} u_{ij}^{n}(\mathbf{x}, \xi)\mathrm{e}^{-\beta_n t} \tag{A15}$$

where

$$u_{ij}^{n}(\mathbf{x}, \xi) = \gamma_n f_{ij}(\mathbf{x}, \xi) + \chi_n g_{ij}(\mathbf{x}, \xi) \tag{A16}$$

All other time-dependent viscoelastic fundamental solutions for traction, stress and strain components can be obtained in the same form by the same procedure. In particular, the fundamental solution for traction can be expressed in the form

$$p_{ij}^{*}(\mathbf{x}, \xi; t) = [\delta_{1\alpha}\delta(t) + \delta_{2\alpha}]p_{ij}^{0}(\mathbf{x}, \xi) + \sum_{m=1}^{M} p_{ij}^{m}(\mathbf{x}, \xi)\mathrm{e}^{-\alpha_m t} \tag{A17}$$

Appendix B. Convolution quadrature

A convolution integral $y(t) = f(t) * g(t)$ can be numerically approximated by the finite sum

$$y(n\Delta t) = \sum_{k=0}^{n} \omega_{n-k}(\Delta t) g(k\Delta t), \qquad n = 0, 1, \ldots, N$$

where the quadrature weights ω_n are the coefficients of the power series

$$\bar{f}\left[\frac{\gamma(z)}{\Delta t}\right] = \sum_{m=0}^{\infty} \omega_m(\Delta t) z^m \tag{B1}$$

and $\gamma(z)$ is a complex polynomial function, which needs to satisfy certain stability conditions. Lubich suggests as appropriate choice for $\gamma(z)$ the P-order backward differentiation formula

$$\gamma(z) = \sum_{m=1}^{P} \frac{1}{m}(1 - z)^m, \qquad P = 1, 2, \ldots 6 \tag{B2}$$

It is clear from Eq. (B1) that ω_n is given by

$$\omega_n(\Delta t) = \frac{1}{2\pi i}\int_C \bar{f}\left[\frac{\gamma(z)}{\Delta t}\right] z^{-n-1} \, \mathrm{d}z \tag{B3}$$

where C is the contour of a circular region of radius ρ within which $\gamma(z)$ is analytic. The integral on the right hand-side of Eq. (B3) can be approximated by a sum, so that

$$\omega_n(\Delta t) \cong \frac{1}{L}\sum_{l=0}^{L-1} \bar{f}\left[\frac{\gamma(\zeta_l)}{\Delta t}\right]\zeta_l^{-n} \tag{B4}$$

where

$$\zeta_l = \rho \exp\left(\frac{2\pi l}{L} i\right)$$

References

[1] Rizzo FJ, Shippy DJ. An application of the correspondence principle of linear viscoelasticity theory. SIAM J Appl Math 1971;21:321–30.

[2] Shinokawa T, Kaneko N, Yoshida N, Kawahara M. Application of viscoelastic combined finite and boundary element analysis to geotechnical engineering. In: Brebbia, Maier, editors. Boundary elements VII, vol. 2. Berlin: Springer; 1985. p. 1037–46.

[3] Schanz M. A boundary element formulation in time domain for viscoelastic solids. Comm Numer Meth Engng 1999;15:799–809.

[4] Gurtin ME, Sternberg E. On the linear theory of viscoelasticity. Arch Rat Mech Anal 1962;11:291–356.

[5] Carini A, De Donato O. Fundamental solutions for linear viscoelastic continua. Int J Solids Struct 1992;29:2989–3009.

[6] Lubich C. Convolution quadrature and discretised operational calculus I. Numer Math 1988;52:129–45.

[7] Lubich C. Convolution quadrature and discretised operational calculus II. Numer Math 1988;52:413–25.

[8] Sim WJ, Kwak BM. Linear viscoelastic analysis in time domain by boundary element method. Comp Struct 1988;29(4):531–9.

[9] Dooling PJ, Buckley CP, Hinduja S. The onset of nonlinear viscoelasticity in multiaxial creep of glassy polymers: a constitutive model and its application to PMMA. Pol Engng Sci 1998;38: 892–904.

[10] Mueller HK, Knauss WG. Crack propagation in a linearly viscoelastic strip. Trans ASME, J Appl Mech 1971;38:483–8.